Direct Estimation of Biological Growth Properties from Image Data Using the "GRID" Model

Nataliya Portman[1], Ulf Grenander[2], and Edward R. Vrscay[1]

[1] Department of Applied Mathematics, University of Waterloo, Waterloo, Ontario, N2L 3G1, Canada
{nportman,ervrscay}@math.uwaterloo.ca
[2] Division of Applied Mathematics, Brown University, Providence, Rhode Island, 02912, USA
ulf-grenander@cox.net

Abstract. Having acquired images of a growing organism, the question arises how they can be used to infer the properties of growth. We address this challenging image understanding problem by using the GRID (Growth as Random Iterated Diffeomorphisms) model for biological growth. In the GRID model, growth patterns are composed of smaller, local deformations, each resulting from elementary biological events (e.g.,cell division). A large number of such biological events, each occurring randomly and independently from one another, results in a visible growth pattern or biological shape changes as seen in images. A biological transformation underlying observed shape changes is a solution to a GRID visible growth differential equation. We propose its automatic generation via direct estimation of the growth magnitudes from image data. The growth magnitude is a GRID parameter that characterizes a local expansion/contraction rate throughout the organism's domain. The estimation algorithm is based on the unconstrained optimal control problem formulation expressed in Darcyan coordinates of the organism's domain and consequent application of Polak-Ribiere minimization routine. We demonstrate the proposed inference method using confocal micrographs of the Drosophila wing disc at larval stage of development.

1 Introduction

Morphological differences between anatomical structures seen in images have been modeled by means of diffeomorphic transformations on the compact background space of Cartesian coordinates. Various techniques for the estimation of smooth deformations that register one image with another have been used in the past. Landmark matching algorithms utilizing thin plate splines [1,2], algorithms using elastic [3,4] and viscous fluid flow [5,6] models of deformations, point-based [7] and curve-based [8] algorithms yield diffeomorphic mappings consistent with the material and geometric properties of the anatomical structure under study.

M. Kamel and A. Campilho (Eds.): ICIAR 2009, LNCS 5627, pp. 832–843, 2009.

In contrast to the existing models of deformations, the Growth as Random Iterated Diffeomorphisms (GRID) model [9,10] introduced by U. Grenander defines complete shape transformations in accordance with fundamental biological principles of growth. A biological transformation that represents growth on a small time scale is a time-varying sequence of several smaller deformations (i.e., local expansions and contractions), each resulting from an elementary cell decision (e.g. division, enlargement). The characterization of such biological growth in terms of such GRID variables as seeds, locations of cell decisions, and local deformation patterns, as well as their estimation have been proposed in [11].

Since the GRID variables define the growth-related deformations, it is desirable to estimate them directly from image data. In this way, we can claim that the underlying transformations estimated from the GRID parameters of growth are biologically meaningful. Our ultimate goal is to develop a systematic approach to infer growth properties expressed by the GRID parameters directly from images. This will give us more insight into the inner workings of a growing organism. In this paper we present an algorithm to estimate the *growth magnitude*, a GRID parameter that measures the local expansion/contraction rate throughout the organism's domain using a simpler, isotropic (i.e., angularly-independent) version of the GRID model. We then employ a macroscopic growth law that represents growth on a large time scale. This is a deterministic integro-differential equation that generates a diffeomorphic flow as a result of an infinite number of elementary biological events at each time instant.

The macroscopic growth law is used to formulate an unconstrained optimal control problem. The growth magnitude is an optimal control that minimizes the squared L^2 distance between the target image of a grown organism and the source image of an initial organism under the transformation. The Polak-Ribiere conjugate gradient (CG) algorithm is then employed for the direct estimation of the growth magnitude GRID parameter from given images. The biological mapping is then automatically obtained from the estimated optimal growth magnitudes. It is important to maintain the diffeomorphic property of the estimated mapping during image registration, so that the growing organism does not overlap itself. It is shown that in order to preserve topology, the estimation algorithm cannot be run to full convergence.

A novel feature of the proposed algorithm is the implementation of *Darcyan biological coordinate systems* [12] to represent the evolving geometry of a growing organism. In comparison to Cartesian grids, Darcyan grids capture not only local deformation patterns but also overall shape changes occurring due to growth. We also show how the Darcyan coordinate system can be used for image registration performed in the image preprocessing step of our estimation algorithm.

In the experiments presented below, we assume that seeds are distributed according to a Poisson point process with constant Poisson intensity parameter throughout the organism's domain. In general, the Poisson intensity parameter is space- and time-dependent. But for some organisms such as the imaginal discs of the Drosophila embryo, time-independent and uniform distribution of seeds that designate cell division locations is a biologically realistic assumption.

2 Biological Background

Confocal microscopy has been gaining popularity in the biological science community for its capability to visualize genes in action in embryos. Gene expression patterns seen in micrographs of the growing Drosophila's wing disc reveal the position and shape of adult wing and body structures long before they actually form [13]. In Figure 1.a is shown the subdivision of the wing disc into the notum and wing subregions, with the latter being separated into the future dorsal and ventral wing surfaces. It evolves as a result of simultaneous temporal and spatial expression patterns of the key regulatory genes required for the wing formation in Drosophila in the late stage of its larval development[14]. The "Wingless protein" plays a major role in patterning of the wing disc. As the wing disc grows the Wingless protein becomes more concentrated near the dorsal/ventral boundary, as seen in Figure 1.b.

The sequence of micrographs (see Fig. 1.b) gives us direct biological data since brightness intensities of the image pixels correspond to the levels of expression of Wingless gene in the cells. We use these data to estimate the underlying growth magnitude and growth-induced transformation and ignore the effects of the 'secondary' regulatory genes, namely, Apterous and Vestigial genes, to avoid additional complexity of the inference problem. Two-dimensional GRID modeling of the larval wing disc growth appears to be natural due to the following biological facts:
(1) Cells divide randomly and uniformly throughout the wing disc at the larval stage of development.
(2) The cell number doubles on average every 9 hours during the second and early third instar.
(3) Most cell movements are due to passive displacements (newborn cells pushing existent ones).
(4) The disc epithelium is one cell thick like the ectoderm.

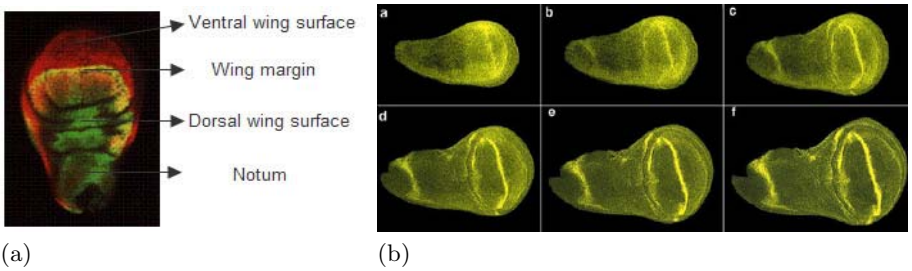

(a) (b)

Fig. 1. (a) Overlapping of the Vestigial and Apterous gene expression patterns, (b) Dynamics of the Wingless gene expression pattern during larval disc growth. First and last micrographs in the sequence correspond to an embryo's age of $\approx$ 48 hours and $\approx$ 120 hours after egg laying. ((a): Courtesy of J. A. Williams, S. W. Paddock and S. B. Carroll, Howard Hughes Medical Institute and Laboratory of Molecular Biology, USA. (b): Courtesy of S. Paddock and D. McDougal, University of Wisconsin, USA.)

3 Isotropic GRID Model and Optimization Problem Formulation Using GRID Macroscopic Growth Law

The spatio-temporal Wingless gene expression pattern is described by an image function $I(x,t)$. $I(x_{ij},t)$ is the brightness intensity of the image pixel x_{ij} at time t corresponding to the concentration level of the Wingless protein in the cell located at x_{ij} . Given a pair of consecutive images $I_1(x(\xi),0)$ and $I_2(x(\xi),T)$ (Fig.2) we wish to infer the growth magnitude $a(\xi)$ and the diffeomorphic transformation $\phi_t(x(\xi),a(\xi))$, $(0 \leq t \leq T)$, by constructing transformations with a least energy property. Such an optimal transformation is controlled by the GRID variable $a(\xi)$. We first estimate $a(\xi)$ directly from given images by minimizing the squared distance between the target image $I_2(x(\xi),T)$ and the source image under the deformation $I_1(\phi_T(x(\xi),a(\xi)),0)$, where $\phi_t(x(\xi),a(\xi))$ is the solution to the macroscopic growth differential equation.

This equation approximates observed growth in instantaneous time as a result of an infinite number of cell decisions that occur randomly and independently in the growing organism's domain. By the Law of Large Numbers the growth increment at each time instant is the average value of the displacement field taken over all seed contributions. According to the isotropic GRID model the displacement field due to a fixed seed contribution, $\theta^{\xi_{seed}}(x)$, is modeled as an exponential decay of the radial distance from the seed:

$$\begin{aligned} \Delta^{\xi_{seed}} x(\xi) &= k(x(\xi)) \cdot (x(\xi) - x(\xi_{seed})) \cdot e^{-\|(x(\xi)-x(\xi_{seed}))\|^2/step(x(\xi_{seed}))^2} \\ &= k(x(\xi_{seed})) \cdot \theta(x(\xi) - x(\xi_{seed})), \end{aligned} \quad (1)$$

where
(1) $x(\xi)$ is a curvilinear Darcyan coordinate system of the organism's domain, where $\xi = (\xi_1, \xi_2)$, ξ_1, ξ_2 are integers, $1 \leq \xi_1 \leq n, 1 \leq \xi_2 \leq m$.
(2) $k(x(\xi))$ is the radial growth/decay constant direction: $0 < k(x(\xi)) < 1$ implies expansion of the small area around $x(\xi)$ and $-1 < k(x(\xi)) < 0$ implies local contraction.

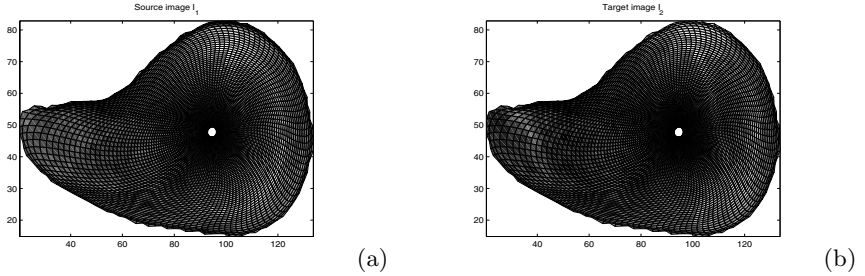

(a) (b)

Fig. 2. (2.a) Source image $I_1(x(\xi),0)$ and (2.b) target image $I_2(x(\xi),T)$ interpolated on the Darcyan grid of the wing disc in I_1

(3) $step(x(\xi_{seed}))$ is the radius of influence of the seed. Since $x(\xi)$ provides a computational grid with non-uniformly distributed nodes, the *step* parameter is set to be the Jacobian of the transformation $x(\xi) = (x_1(\xi_1, \xi_2), x_2(\xi_1, \xi_2))$, i.e., $step(x(\xi)) = |\frac{\partial(x_1,x_2)}{\partial(\xi_1,\xi_2)}|$.

Finally, the macroscopic growth equation is obtained by averaging over all displacement fields.

$$\frac{\partial x(\xi,t)}{\partial t} = \int_{\xi_{seed}\in\Xi} \Delta^{\xi_{seed}} x(\xi) F(d\xi_{seed}) = \int_{\xi_{seed}\in\Xi} k(x(\xi_{seed})) \cdot \theta(x(\xi) - x(\xi_{seed})) \cdot f(x(\xi_{seed}))d\xi_{seed}. \tag{2}$$

Here, $f(x(\xi_{seed}))$ is the Poisson intensity measure underlying seed placements. We stress the fact that this measure of density of cell decisions is defined in absolute space coordinates x which depend on Darcyan coordinates ξ_{seed} of local gene activity sites. By conservation of probability,

$$f(x) = f(x(\xi)) = \frac{\lambda(\xi)}{J(\xi)}, \quad \text{where} \quad J(x(\xi)) = \left|\frac{\partial(x_1,x_2)}{\partial(\xi_1,\xi_2)}\right|. \tag{3}$$

The Poisson intensity measure expressed in Darcyan coordinates $\xi_{seed} \in \Xi$ is an intrinsic growth property of an organism represented by $\lambda(\xi_{seed})$. We introduce a bounded measure $a(\xi_{seed})$ called the *growth magnitude* and defined as follows,

$$a(\xi_{seed}) = k(x(\xi_{seed})) \cdot f(x(\xi_{seed})). \tag{4}$$

Since cells divide uniformly in the Drosophila's wing disc, the Poisson intensity $\lambda(\xi_{seed})$ is assumed to be a uniform probability density function. This knowledge is incorporated into the macroscopic growth model as follows,

$$a(\xi_{seed}) = \frac{k(x(\xi_{seed}))}{J(\xi_{seed})}. \tag{5}$$

We are led to the following unconstrained optimal control problem for estimation of the growth magnitude $a(\xi)$ and the corresponding biological transformation $\phi_T(x(\xi), a(\xi))$:

$$\hat{a} = \arg\min_{a\in L^\infty} \int_\Xi (I_2(x(\xi), T) - I_1(\phi_T(x(\xi), a(\xi)), 0)^2 \left|\frac{\partial(x_1,x_2)}{\partial(\xi_1,\xi_2)}\right| d\xi, \tag{6}$$

subject to

$$\frac{\partial \phi_t(x(\xi), a(\xi))}{\partial t} = \int_{\xi_{seed}\in\Xi} \theta(\phi_t(x(\xi), a(\xi)) - x(\xi_{seed})) \cdot a(\xi_{seed}, t)\, d\xi_{seed}, \tag{7}$$

with initial conditions, $\phi_0(x(\xi), a(\xi)) = x(\xi)$, $a(\xi) = 0$.

4 An Algorithm for Direct Estimation of the Growth Magnitude from Image Data

In order to solve the optimization problem for $\hat{a(\xi)}$ we state its space-time discretized version,

$$\hat{a} = \arg\min_{a \in L^\infty} \sum_{\xi_j \in \Xi} (I_2(x(\xi_j), T) - I_1({\phi^{-1}}_T(x(\xi_j), a(\xi_j)), 0))^2 \left| \frac{\partial(x_1, x_2)}{\partial(\xi_{1_j}, \xi_{2_j})} \right|, \quad (8)$$

subject to

$$\phi_T(x(\xi_i), a(\xi_i)) = x(\xi_i) + \sum_{t=1}^{T} \sum_{\xi_{seed_j} \in \Xi} \theta(\phi_t(x(\xi_i), a(\xi_i)) - x(\xi_{seed_j}, t)) \cdot a(\xi_{seed_j}) \quad (9)$$

for all seeds ξ_i, $1 \leq i \leq M$.

We implement the following steps of the estimation algorithm:

Step 1. Construction of the Darcyan coordinate system of the wing disc seen in I_1 and I_2 using the Level Set Method as described in [12].Since there is no difference in the grey level contents of both images in the neighborhood of the Darcyan origin we stop propagating the level sets into this area. The resulting Darcyan grid contains 80 radial and 120 angular coordinate lines. Since the image function I is defined on a rectangular uniform lattice we apply bilinear interpolation to estimate image values at the nodes of the curvilinear Darcyan coordinate system $I(x(\xi_i))$, where $1 \leq i \leq M$ (Fig.2).

Step 2. Image preprocessing.

(i) Image registration about the origin of Darcyan coordinate system applying Principal Component Analysis (PCA). We remove the rigid transformation from the observed images using Darcyan coordinate representations of the initial and grown wing discs. Given the Darcyan grid nodes $x_i = x(\xi_{1_i}, \xi_{2_i}), , 1 \leq i \leq M$, we define the covariance matrix $K = \frac{1}{M} \sum_{n=1}^{M} \{(x_i - x_c)(x_i - x_c)^T\}$ and its eigenvectors for I_1 and I_2. Here, x_c is the origin of the Darcyan coordinate system of the grown wing disc shown in I_2 (Fig.3.b). The eigenvectors of K give the principal axes of both Darcyans. I_1 and I_2 are registered by aligning these principal axes (Fig.3.a).

(ii) Reduction of salt and pepper noise, which is inherent to confocal microscopy. A median filter using a 3×3 window can be applied since it has a property of reducing this kind of noise while preserving edges.

Step 3. Realization of the conjugate gradient method to find the optimal value of the growth magnitude $\hat{a(\xi)}$. We have chosen the Polak-Ribiere version [15] since it is useful in finding the minimum of a nonconvex function in R^M: the repeated cycles of M iterations eventually converge to the minimum. We construct a minimizing sequence of optimal controls $\{a(\xi, t_i)\}_{i=1}^{N}$ such that $\lim_{t \to t_N} a(\xi, t) = \hat{a}(\xi)$ and $I_2(x(\xi), t_N) \approx I_1({\phi^{-1}}_{t_N}(x(\xi), \hat{a(\xi)}), 0)$. Denoting an evolving Darcyan

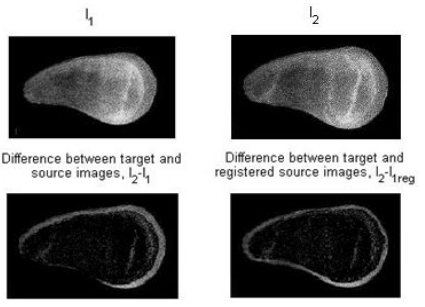

(a)

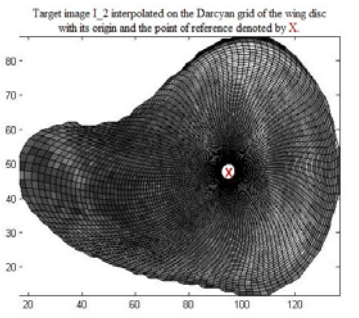

(b)

Fig. 3. (3.a) $I_2(x) - I_1(x)$ before and after registration, (3.b)$I_2(x(\xi), T)$ interpolated on the Darcyan grid of the wing disc with its origin and point of reference for registration denoted by **X**

coordinate system of the wing disc by $x(\xi, t_i) = \phi_{t_i}(x(\xi), a(\xi))$ we compute the energy gradient,

$$\nabla E(a(\xi, t_i)) = \nabla_a(\sum_{\xi_j \in \Xi}(I_2(x(\xi_j), T) - I_1(x^{-1}(\xi_j, t_i), 0))^2 |\frac{\partial(x_1, x_2)}{\partial(\xi_{1_j}, \xi_{2_j})}|),$$

where the Darcyan grid is updated at each t_i as follows,

$$x(\xi, t_i) = x(\xi, t_{i-1}) + \sum_{\xi_{seed_j} \in \Xi} \theta(x(\xi_i, t_{i-1}) - x(\xi_{seed_j}, t_{i-1})) \cdot a(\xi_{seed_j}, t_i). \quad (10)$$

5 Computational Aspects of the Estimation Algorithm

At each iteration of the Polak-Ribiere procedure we must minimize the energy functional $E(a(\xi, t_i))$ along the direction $h_i \in R^M$ conjugate to all previous directions. We solve a one-dimensional line minimization problem,

$$\lambda_i = \arg\min_{\lambda > 0} E(a(\xi, t_i) + \lambda \cdot h_i(\xi)), \quad (11)$$

which appears to be non-trivial when the behavior of $E(a(\xi, t_i))$ is unknown. It is tempting to approximate the energy functional as a function of λ by a high-order interpolating polynomial but this approach does not guarantee right interpolation. As such, we have employed a Golden Section-based algorithm of one-dimensional minimization [16] that first brackets the local minimum and then isolates it using the signs of the energy derivative on both sides of the minimum. The zeroth value of λ yielded by this code is used as a stopping criterion for the multidimensional minimization. Indeed, in this case E attains its minimum at the previous value of λ_i. The implementation of such a 1D minimization routine is done with an increase in computational time but with a corresponding increase in precision of the image estimates.

6 GRID Characterization of Drosophila Wing Disc Growth

Using consecutive pairs of images in a given sequence of micrographs (Fig.1.b), we apply our estimation algorithm on a Darcyan grid of size 120×80 representing the wing disc at a certain age. A comparison of the estimated target images in Figures 4.h-4.i and 5.n-5.o and the corresponding target images shown in Figures 4.d-4.f and 5.l-5.m shows that the estimated biological transformation $\phi_T(x(\xi), a(\hat{\xi})$ does not fully register images. It tends to flatten subregions of high contrast such as the dorsal part of the wing disc with a strip of a high concentration of Wingless protein observed in target images. In the estimated images of the wing disc in the late stage of larval development (Fig.5.n and 5.o) the boundaries of this strip appear blurry. However, the algorithm performs well in subregions with the highest mismatch of grey levels, such as the area near the tip of the anterior part of the wing disc, seen as a black band in the source image (Fig. 4.a) and as a light gray band in the corresponding target image (Fig. 4.d).

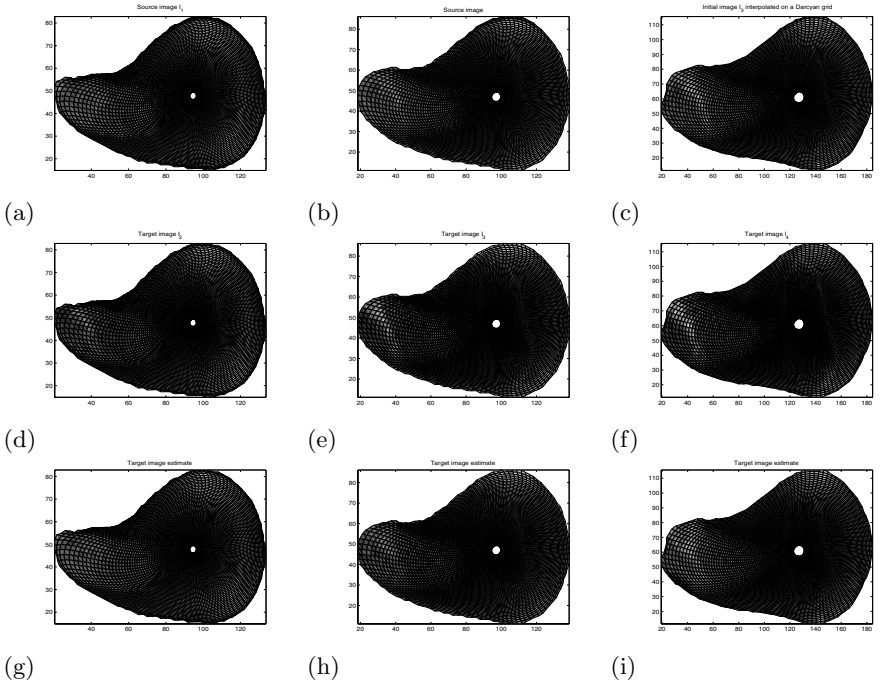

Fig. 4. (4.a-4.c) Source images of the Drosophila wing disc $I_1(x(\xi))$, $I_2(x(\xi))$, $I_3(x(\xi))$, (4.d-4.f) Target images of the wing disc $I_2(x(\xi))$, $I_3(x(\xi))$, $I_4(x(\xi))$, (4.g-4.i) Estimates of target images $I_1(x^{-1}(\xi, T))$, $I_2(x^{-1}(\xi, T))$, $I_3(x^{-1}(\xi, T))$

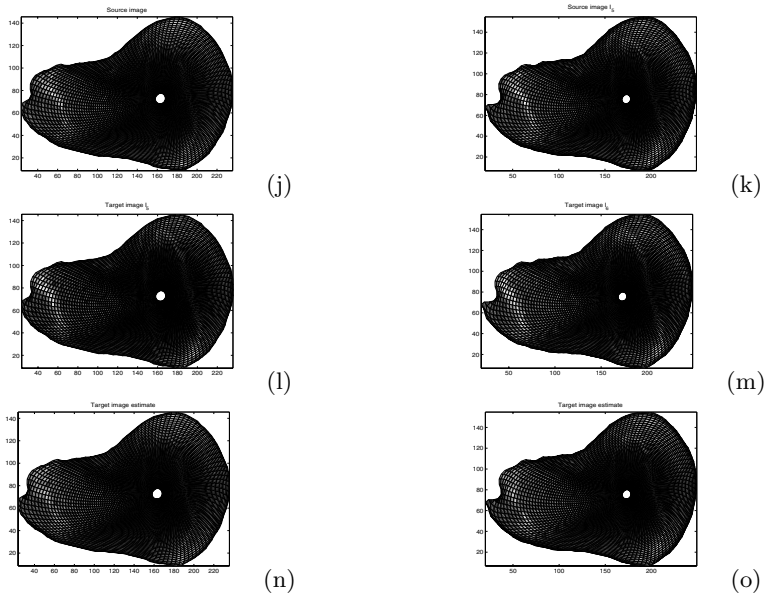

Fig. 5. (5.j-5.k) Source images of the Drosophila wing disc $I_4(x(\xi))$, $I_5(x(\xi))$, (5.l-5.m) Target images of the wing disc $I_5(x(\xi))$, $I_6(x(\xi))$, (5.n-5.o) Estimates of target images $I_4(x^{-1}(\xi,T))$, $I_5(x^{-1}(\xi,T))$

Full convergence of the Polak-Ribiere minimization algorithm has been achieved in the experiments registering images I_1 and I_2, I_2 and I_3, I_3 and I_4. We certainly cannot claim that the optimal growth magnitude, in particular, the k-function shown by a color-coded plot in Figures 6.a-6.c, is the global minimizer of the energy functional. With the initial guess of the zeroth value for the growth magnitude we expect to find an estimate close to zero throughout the whole domain of the wing disc. Small values of $a(\hat{\xi})$ preserve integrity of the Darcyan grid.

For the problem of registering images of the wing disc at a later stage of larval development, the results of only three iterations of the CG algorithm have been presented in Figures 7.j-7.k. Additional iterations of the Polak-Ribiere procedure cause local overlaps of the cellular field presented by its Darcyan grid with locally intersecting radial grid lines. We also observe that the estimated k-function oscillates wildly throughout the interior of the wing disc. This is the consequence of unconstrained optimization.

A combination of regions of contraction and expansion shown in blue and red in Figures 6.a-6.c and 7.j-7.k, respectively, is biologically meaningful. This distribution can describe growth with regions in red designating cell division locations. It is possible that the dividing cells push out the neighboring cells causing local contractions of the cellular field. This growth mode is also captured by the Darcyan coordinate system deformed under the estimated growth-induced transformation, as shown in Figures 6.d-6.f and 7.l-7.m.

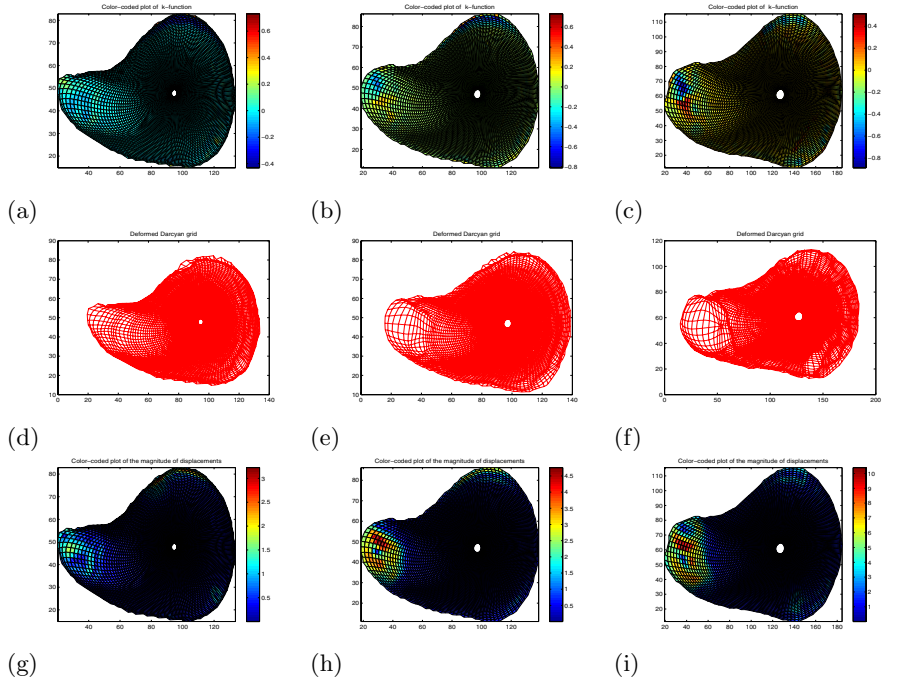

Fig. 6. (6.a-6.c)Color-coded plot of the optimal local expansion/contraction rate $k(\xi)$ for image pairs $(I_1,\ I_2)$, $(I_2,\ I_3)$, $(I_3,\ I_4)$, (6.d-6.f) Deformed Darcyan grid of the wing disc given in $I_1(x(\xi))$, $I_2(x(\xi))$, $I_3(x(\xi))$ generated by the estimated biological transformation, (6.g-6.i) Color-coded plot of the magnitude of the displacements for image pairs $(I_1,\ I_2)$, $(I_2,\ I_3)$, $(I_3,\ I_4)$

The magnitude of the displacement field $\parallel \Delta x(\xi) \parallel = \parallel x(\xi, T) - x(\xi, 0) \parallel$ shown in Figures 6.g-6.i and 7.n-7.o reveals a spatial-temporal deformation pattern with displacements concentrated near the tip of the anterior part of the wing disc in the early larval stage. As time progresses it evolves into a deformation pattern of high concentration in the dorsal region with the appearance of local deformation effects in the posterior part. This is consistent with the deformed Darcyan grid of the growing wing disc undergoing large expansions near the tip of the dorsal region. This suggests that the dorsal part of the wing disc grows faster during larval development.

7 Summary and Future Directions

We have outlined an algorithm to estimate the growth magnitude GRID variables directly from image data. With the assumption of uniform space-time probability distribution of cell decisions, the growth magnitude represents a local rate of contraction/expansion throughout the domain of a growing organism. Using image data from the larval development of the Drosophila wing disc, we

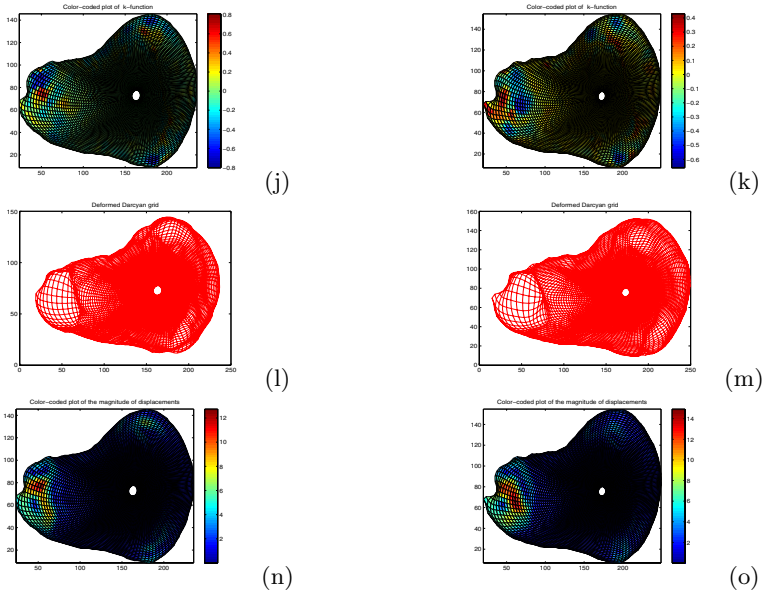

Fig. 7. (7.j-6.k) Color-coded plot of the optimal local expansion/contraction rate $k(\xi)$ for image pairs (I_4, I_5), (I_5, I_6), (7.l-7.m) Deformed Darcyan grid of the wing disc given in $I_4(x(\xi))$, $I_5(x(\xi))$ generated by the estimated biological transformation $x(\xi, t)$, $0 \leq t \leq T$, (7.n-7.o) Color-coded plot of the magnitude of the displacements for image pairs (I_4, I_5) and (I_5, I_6)

have shown that the algorithm yields biologically meaningful inferences of the growth-induced deformations.

However, our algorithm does not fully register images of the Wingless gene expression patterns of the growing wing disc. Moreover, the proposed algorithm cannot generally be run to full convergence since the preservation of the organism's topology is not guaranteed. Currently, we are examining a number of directions in order to improve the performance of the algorithm:

(1) **Analysis of the macroscopic growth integro-differential equation.** We consider the macroscopic growth equation written as $\Delta x = \Theta \cdot a$, where $\Theta(z) = zexp(-\frac{\|z\|^2}{step^2})$ with $z = x(\xi) - x(\xi_{seed})$. We are studying the numerical stability of the inverse problem $a = \Theta^{-1}\Delta x$.

(2) **Modification of the proposed cost function.** We assume that the discretized $a(\xi)$ is a sample from the multivariate Gaussian distribution. The cost function will contain an additional penalty term $E_{penalty} = 1/2{\sigma_a}^2 \parallel a(\xi) \parallel^2$ which attempts to preserve the topology of a growing organism.

(3) **Direct estimation of non-uniform Poisson intensity parameter.** We consider the case of the non-uniform probability density and define the absolute value of the unknown a-field as the Poisson intensity measure. We seek a penalty function that measures cell activities driving observed growth deformations.

Acknowledgements

This research was supported in part by the Natural Sciences and Engineering Research Council of Canada (NSERC), in the form of a Postgraduate Scholarship (NP) and a Discovery Grant (ERV).

References

1. Bookstein, F.L.: Morphometric Tools for Landmark Data: Geometry and Biology. Cambridge University Press, Cambridge (1991)
2. Bookstein, F.L.: Biometrics, Biomathematics and the Morphometric Synthesis. Bull. of Math. Biol. 58(2), 313–365 (1996)
3. Davatzikos, C.: Spatial Transformation and Registration of Brain Images Using Elastically Deformable Models. Comput. Vision Image Under. 66(2), 207–222 (1997)
4. Kyriacou, S.K., Davatzikos, C., Zinreich, S.J., Bryan, R.N.: Nonlinear Elastic Registration of Brain Images with Tumor Pathology Using Biomechanical Model. IEEE Trans. Med. Imaging 18(7), 580–592 (1999)
5. Christensen, G.E., Rabbitt, R.D., Miller, M.I.: A Deformable Neuroanatomy Textbook Based on Viscous Fluid Mechanics. In: Proceedings of 1993 Conf. on Information Sciences and Systems, Johns Hopkins University, pp. 211–216 (1999)
6. Christensen, G.E., Sarang, C.J., Miller, M.I.: Volumetric Transformation of Brain Anatomy. IEEE Trans. Med. Imaging 16(6), 864–876 (1997)
7. Bookstein, F.L.: Size and Shape Spaces for Landmark Data in Two Dimensions. Statistical Science 1, 181–242 (1998)
8. Khaneja, N., Miller, M., Grenander, U.: Dynamic Programming Generation of Curves on Brain Surfaces. IEEE Trans. Patt. Anal. Mach. Int. 20(11), 1260–1264 (1998)
9. Srivastava, A., Saini, S., Ding, Z., Grenander, U.: Maximum-Likelihood Estimation of Biological Growth Variables. In: Rangarajan, A., Vemuri, B.C., Yuille, A.L. (eds.) EMMCVPR 2005. LNCS, vol. 3757, pp. 107–118. Springer, Heidelberg (2005)
10. Grenander, U.: On the Mathematics of Growth. Quart. Appl. Math. 65, 205–257 (2007)
11. Grenander, U., Srivastava, A., Saini, S.: A Pattern-Theoretic Characterization of Biological Growth. IEEE Trans. Med. Imaging 26(5), 648–659 (2007)
12. Portman, N., Grenander, U., Vrscay, E.R.: New computational methods for the construction of "Darcyan" biological coordinate systems. In: Kamel, M.S., Campilho, A. (eds.) ICIAR 2007. LNCS, vol. 4633, pp. 143–156. Springer, Heidelberg (2007)
13. Carroll, S.B.: Endless Forms Most Beautiful: The New Science of Evo Devo and the Making of the Animal Kingdom. W. W. Norton & Company, NY (2005)
14. Williams, J.A., Paddock, S.W., Carroll, S.B.: Pattern Formation in a Secondary Field: a Hierarchy of Regulatory Genes Subdivides the Developing Drosophila Wing Disc into Discrete Subregions. Development 117, 571–584 (1993)
15. Polak, E.: omputational Methods in Optimization: a Unified Approach. Mathematics in Science and Engineering, vol. 77. Academic Press, NY (1971)
16. Press, W.H., Flannery, B.P., Teukolsky, S.A., Vetterling, W.T.: Numerical Recipes in C: The Art of Scientific Computing. Cambridge University Press, Cambridge (1992)